Strain Mapping in a Graphene Monolayer Nanocomposite

Robert J. Young,[†,*] Lei Gong,[†] Ian A. Kinloch,[†] Ibtsam Riaz,[‡] Rashed Jalil,[‡] and Kostya S. Novoselov[‡]

[†]Materials Science Centre, School of Materials and [‡]School of Physics and Astronomy, University of Manchester, Oxford Road, Manchester M13 9PL, U.K.

ABSTRACT Model composite specimens have been prepared consisting of a graphene monolayer sandwiched between two thin layers of polymer on the surface of a poly(methyl methacrylate) beam. It has been found that well-defined Raman spectra can be obtained from the single graphene atomic layer and that stress-induced Raman band shifts enable the strain distribution in the monolayer to be mapped with a high degree of precision. It has been demonstrated that the distribution of strain across the graphene monolayer is relatively uniform at levels of applied strain up to 0.6% but that it becomes highly nonuniform above this strain. The change in the strain distributions has been shown to be due to a fragmentation process due to the development of cracks, most likely in the polymer coating layers, with the graphene remaining intact. The strain distributions in the graphene between the cracks are approximately triangular in shape, and the interfacial shear stress in the fragments is only about 0.25 MPa, which is an order of magnitude lower than the interfacial shear stress before fragmentation. This relatively poor level of adhesion between the graphene and polymer layers has important implications for the use of graphene in nanocomposites, and methods of strengthening the graphene–polymer interface are discussed.

KEYWORDS: graphene · Raman spectroscopy · deformation · nanocomposites · micromechanics

Graphene was first isolated in 2004,[1,2] and since that time much effort has been expended in undertaking research into exploiting its electronic properties for applications such as in electronic devices.[3–5] Interest in the material has now broadened considerably, as it was soon realized that graphene might have other interesting physical properties such as high levels of thermal conductivity,[6] stiffness, and strength,[7] coupled with impermeability to gases.[8] One obvious application is in the field of nanocomposites, and a number of detailed studies have already been undertaken on the incorporation of graphene into polymer matrixes.[9] Although many of the papers report work on graphene-reinforced nanocomposites, most have used graphene oxide, often in its reduced form.[10–12] This material can be readily obtained by exfoliating graphite with strong acids,[13] a process known for over 140 years[14] (the material was originally termed "graphite oxide"). It can be reduced chemically toward a material that is closely related to graphene but is by no means perfect and has a significant oxygen content and reactive functional groups on the surface.[15,16]

The authors have recently undertaken the first fundamental study of stress transfer from a polymer matrix to single atomic layers of exfoliated graphene.[17] They demonstrated that stress transfer takes place through shear at the graphene polymer interface and that continuum mechanics still appears to be valid at the atomic level. The shear-lag model used widely to interpret the micromechanics of fiber-reinforced composites[18,19] was shown to be applicable for atomic layers of graphene reinforcing a polymer matrix.

This previous study[17] concentrated on using Raman spectroscopy[20–23] to monitor the variation of axial strain along a line across a single graphene monolayer, both parallel and perpendicular to the axis of matrix tensile strain. In this present study we have mapped the strain in a graphene exfoliated monolayer at different levels of matrix strain for both a free-standing graphene monolayer on a polymer surface and the monolayer sandwiched between thin layers of polymer. This has enabled the level of stress transfer to be evaluated across the entire monolayer and phenomena such as breakdown of the graphene–polymer interface to be followed.

RESULTS AND DISCUSSION

An optical micrograph of the graphene monolayer on a polymer beam before deformation and spin-coating with the top layer of SU-8 is shown in Figure 1. The long axis of the monolayer is aligned approximately parallel to the axis of tensile deformation (horizontal).

The graphene monolayer gave a well-defined Raman spectrum characteristic of single layer graphene with a strong 2D (or G′) band,[24,25] a G band of around half the intensity of the 2D band, and no D band (see Supporting Information). It was found that the 2D band shifted significantly as the beam was deformed in bending, as shown

* Address correspondence to robert.young@manchester.ac.uk.

Received for review January 19, 2011 and accepted March 11, 2011.

Published online March 11, 2011
10.1021/nn2002079

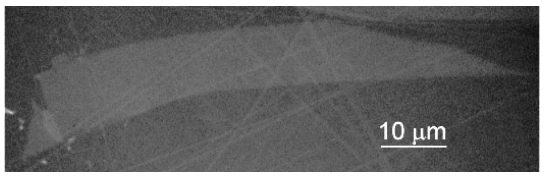

Figure 1. Optical micrograph of the graphene monolayer before deformation. (The faint straight lines in the background are from scratches on the PMMA beam.)

in Figure 2. The shift rate (in terms of strain) was found to be $-61 \pm 2\ \mathrm{cm}^{-1}$/%, which is similar, but not identical, to that found by ourselves[17] and others in previous studies,[20−23] showing good stress transfer between the underlying polymer and graphene monolayer.

It was found that as well as showing a large stress-induced band shift the 2D Raman band also underwent significant broadening during deformation (see Supporting Information). It has been found recently that the 2D band can undergo broadening or even splitting depending on the angle between the axis of laser polarization and high-symmetry directions in the graphene.[23] It has been suggested that this could account for some of the discrepancies between band shift rates measured by different groups.[17,20−23] All of the measurements in this present study, however, were undertaken with the axis of laser polarization parallel to the strain axis in the same direction in the graphene monolayer. Hence the slope of the line in Figure 2 could be used as a calibration for the subsequent mapping of strain in the monolayer without needing to know the exact orientation of the symmetry axes in the graphene monolayer.

Figure 3 shows contour maps of the strain in the graphene monolayer at different levels of strain applied in the horizontal direction along with a key showing the relationship between the contour colors and graphene strain. It was not always possible to make measurements close to the edge of the graphene due to the size of the laser spot (~2 μm), and so the outline of the flake (see Figure 1) is also given in each plot. The black dots also represent the points at which the measurements were taken.

The first two contour plots show the strain maps for applied strains of 0% (i.e., undeformed) and 0.4% for graphene on the PMMA beam before the SU-8 top coating was applied. It can be seen that in both cases the strain in the graphene is relatively uniform with some evidence of a lower strain at the left-hand end at 0.4% strain. This is confirmed in Figure 4a, which shows the distribution of strain over a linear region along the middle of the long axis of the monolayer. It shows that before deformation the strain in the graphene is approximately zero and at 0.4% strain it is uniform along the middle of the monolayer, falling away at the left-hand end and rising higher at the right-hand end.

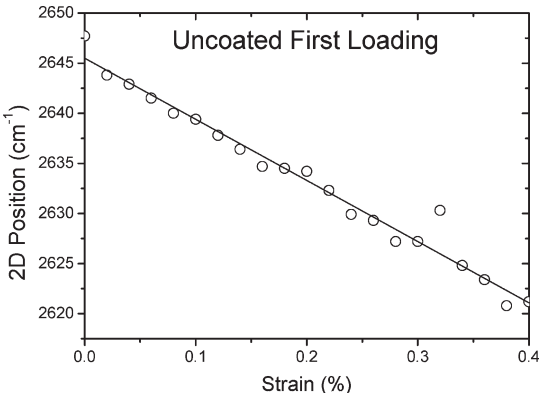

Figure 2. Position of the 2D (G′) Raman band in the uncoated graphene as a function of strain on the beam.

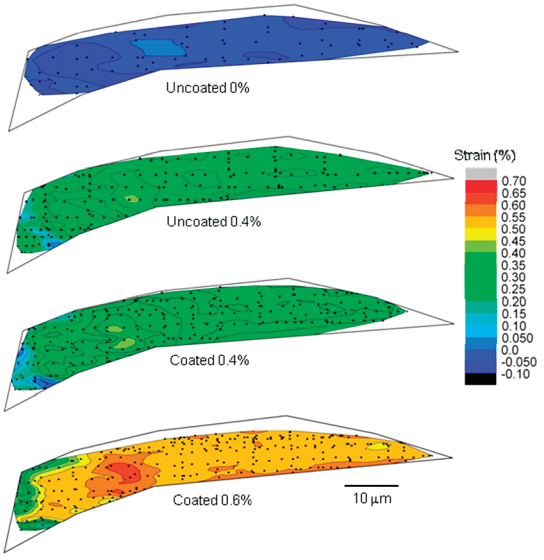

Figure 3. Contour maps of strain over the graphene monolayer at different levels of strain in the uncoated and coated states.

The specimen was unloaded, coated with SU-8, and reloaded to 0.4% and 0.6% strain, and contour maps are also shown in the loaded states following coating in Figure 3. It can be seen that at 0.4% strain the graphene strain distribution is virtually identical in both the uncoated and coated contour maps. This is confirmed in Figure 4b, where there is still a lower level of strain at the left-hand end of the graphene monolayer at 0.4% applied strain following coating. Increasing the applied strain to 0.6% strain causes the strain in the graphene to increase to around 0.6% strain over most of the monolayer, with a lower level of strain at the left-hand end.

The drop off strain at the left-hand end of the monolayer is similar to the behavior reported previously[17] for a graphene monolayer in a model composite under stress. Different behavior is found at the right-hand (pointed) end, and it is possible to obtain some indication of what might be happening in the monolayer from the consideration of the deformation

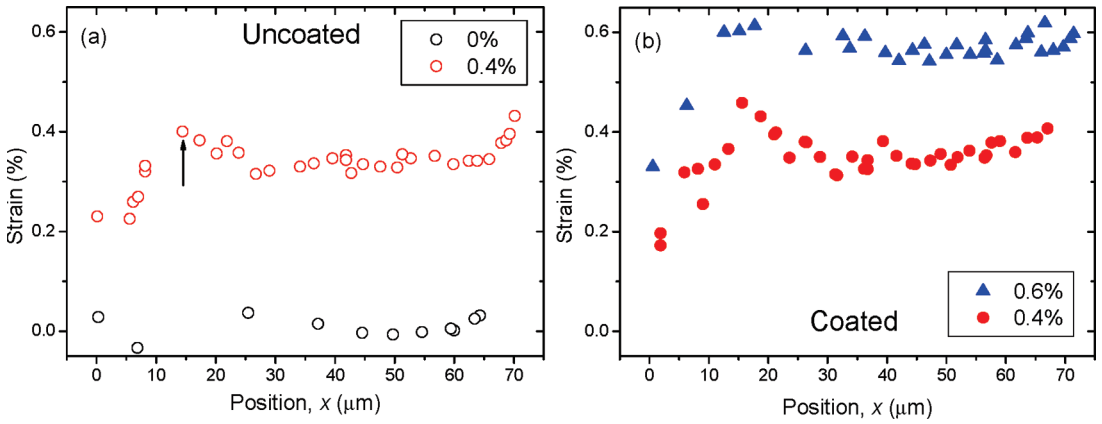

Figure 4. Variation of the strain in the graphene along the middle of the long axis of the monolayer shown in Figure 3, both undeformed (0%) and at a strain of 0.4%. (a) Specimen uncoated and (b) following coating with an SU-8 film. (The arrow indicates the point on the monolayer at which the calibration measurements were undertaken.)

micromechanics of fibers in composites with differently shaped ends.[26,27] In the case of a square end in a cylindrical fiber there is a gradual decrease of fiber strain toward the end of the fiber, as is found at the left-hand end of the monolayer. In contrast, if the fiber has a pointed (e.g., conical) tip, then for high-modulus reinforcements the strain actually rises as the fiber tapers and drops to zero only very close to the end of the tip. The increase in strain seen in Figure 4 at the right-hand tip of the tapering monolayer may take place for a similar reason.

The specimen was unloaded from 0.6% strain, and it was found that there was a residual strain on the order of 0.15% due to creep of the PMMA beam that had occurred under the long period of loading needed to undertake the extensive strain mapping. This manifested itself as a residual curvature of the beam and did not appear to be due to any permanent deformation of the graphene composite. The coated specimen was then reloaded to an applied strain of 0.8%, and Figure 5 shows the variation of the 2D band position, measured at the point indicated by the arrow in Figure 4a, as a function of strain. The reloading data are represented by the solid points, and it can be seen that the slope of the reloading line is similar to that of the initial loading line shown in Figure 2. The data fall close to the line up to about 0.76% strain, at which point the last two data points fall back to the 2D band starting position. This corresponds to the collapse of stress transfer to the graphene monolayer through the interfaces with the polymer films on the beam.

Further information upon stress transfer to the graphene monolayer at higher strain can be gleaned from the contour maps of the strain of the graphene shown in Figure 6. The strain is relatively uniform at around 0.15% in the relaxed state, but when the applied strain is increased to 0.8%, it can be seen that the strain distribution becomes very nonuniform in the graphene monolayer. In particular there are three vertical regions of high strain across the monolayer,

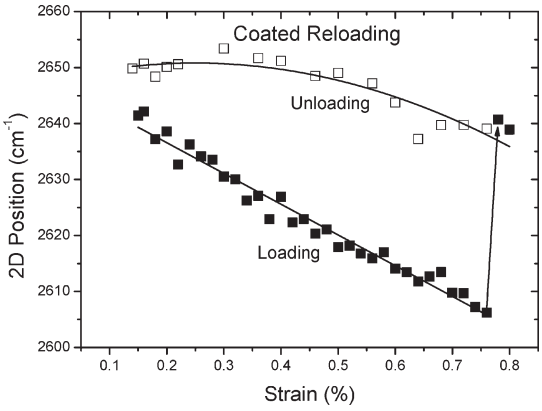

Figure 5. Position of the 2D (G′) Raman band in the coated graphene as a function of strain on the beam during reloading to 0.8% strain and unloading.

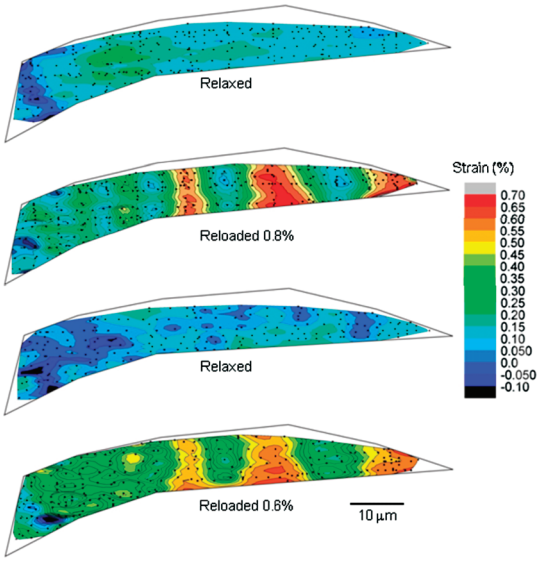

Figure 6. Contour maps of strain over the coated graphene monolayer in the relaxed states and reloaded to 0.8% and 0.6% strain.

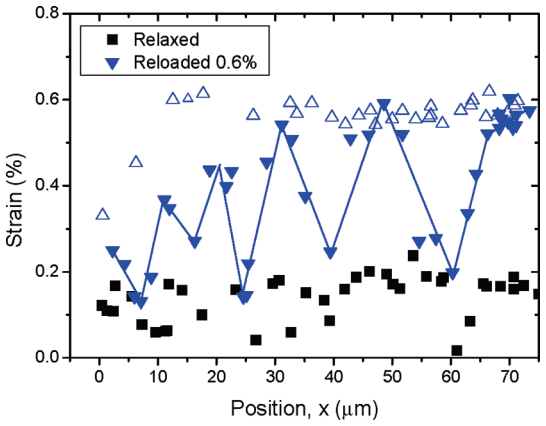

Figure 7. Variation of graphene strain along the middle of the monolayer relaxed and reloaded to 0.6%. (The open triangles are the data points at 0.6% strain for the first loading in Figure 4b.)

with other areas being subjected to lower levels of strain.

Figure 7 shows the variation of strain along the middle of the long axis of the graphene monolayer in the relaxed state and at 0.6% applied strain. The plot confirms that the monolayer is subjected to a relatively uniform strain of around 0.15% in the relaxed state, as shown in Figure 6. When the applied strain is increased to 0.6%, it can be seen that the strain distribution becomes very nonuniform with a series of approximately triangular segments with the strain falling to around 0.2% between each one. The lengths of the segments are in the range 10−20 μm.

Figure 6 shows that when the specimen is relaxed again, the strain falls to around 0.1% but is rather less uniform than when it was relaxed originally. On further reloading to 0.6%, it can be seen that the strain is again nonuniform and the strain pattern is similar to that seen for the specimen when it was loaded to 0.8%. It appears that the specimen was damaged by loading up to 0.8% strain, and this damage was retained on reloading to the lower strain. It should be noted that when the specimen was loaded initially to 0.6% strain, the distribution of strain across the monolayer was relatively uniform (Figure 3), as can be seen from the open triangles in Figure 7.

It is clear from Figures 6 and 7 that loading to 0.8% strain causes damage to the interface between the graphene and polymer layers in the specimen. Figure 8 shows a schematic diagram of the model composite specimen and two possible damage mechanisms:

- fragmentation of the graphene monolayer or
- cracking of the SU-8 coatings

The strain distributions for the graphene monolayer obtained in Figures 6 and 7 would be consistent with either of these two processes taking place.

In order to understand the damage mechanism, the surface of the specimen was examined in a transmission optical microscope. A micrograph of the specimen

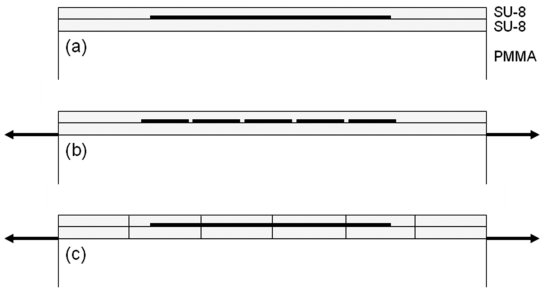

Figure 8. Schematic diagrams of the deformation of the graphene monolayer in a section through the model composite. (a) Specimen before deformation, (b) graphene monolayer undergoing fragmentation, and (c) cracking of both SU-8 polymer coating layers (diagrams not to scale).

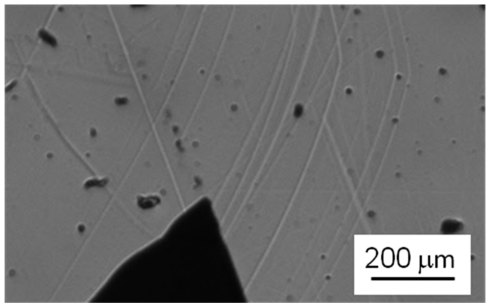

Figure 9. Optical micrograph of the specimen after deformation showing the formation of cracks in the coating that developed during loading. (The tensile axis was horizontal and the large black object at the bottom is a multilayer flake.)

is shown in Figure 9, and it can be seen that there is a network of cracks (or possibly crazes) over the specimen surface; these cracks were not present in the specimen before deformation. The spacing of the cracks in the specimen is on the order of 20 μm and consistent with the pattern of deformation seen in Figure 7. Similar cracks are seen on the surface of the specimen following deformation (see Supporting Information). It appears therefore that the cracks developed during deformation, although it is not possible to tell if they are only in the coated polymer layers or extend into the surface of the PMMA beam. The craze strain of bulk PMMA is over 1%,[28] and so it is most likely that cracking took place just in the SU-8 coatings. Hence it appears that the failure mechanism is that shown in Figure 8c. The fracture stress of monolayer graphene is in excess of 100 GPa and the failure strain over 20%,[7] and so it is unlikely that the graphene monolayer would have fractured at an applied strain of only 0.8%.

The pattern of deformation seen at high strains in Figure 7 is reminiscent of that obtained during the fragmentation test with single-fiber composites.[29,30] In the case of fiber composites it is the fiber that undergoes failure rather than the matrix. It is possible, however, to use the same approach to estimate the shear stress, τ_i, at the interface between the graphene and polymer by assuming that the shear stress at the interface is

balanced by the variation of strain, e_g in the graphene monolayer, with distance along the fragments, x, using the equation[17]

$$\frac{de_g}{dx} = -\frac{\tau_i}{E_g t} \quad (1)$$

where t is the thickness of the graphene and E_g is its Young's modulus. The slopes of the lines in Figure 7 are all very similar and lead to a value of interfacial shear stress on the order of 0.25 MPa, using a Young's modulus E_g of 1050 GPa for the graphene and a thickness t of 0.34 nm for the graphene.

It appears that the fragmentation process completely destroys the interfacial adhesion between the graphene and the polymers. Our previous study[17] showed that the initial level of interfacial shear stress in a similar specimen was on the order of 2 MPa but fell significantly once a triangular-shaped strain distribution developed at higher strain, again probably due to cracking of the polymer layers.

It is interesting to speculate why these values of interfacial shear stress for graphene monolayers in a polymer matrix are significantly lower than those of 20−40 MPa measured for carbon fibers.[29,30] The graphene is atomically smooth, and the interactions can only be van der Waals in character. Computer simulations[31] and modeling[32] of the failure of graphene−polymer interfaces in shear predict values of interfacial shear strength on the order of 100 MPa. Although these values are unrealistic since the polymer matrix will undergo shear yielding at around 50 MPa,[28] there is clearly a discrepancy between the measured and predicted values. It is known that graphene surfaces can easily become contaminated with hydrocarbons and other matter in air.[33] This contamination may be one of the factors that is responsible for the poor adhesion of graphene with polymers.

Although the presence of holes and defects[34,35] leads to graphene oxide having mechanical properties that are significantly inferior to those of graphene,[36,37] the presence of functional groups on the surface[16] may offer better interaction with matrix polymers, particularly if they contain reactive groups such as in the case of epoxy resins. Significant levels of reinforcement have been reported in bulk composites reinforced with graphene oxide,[9] and graphene oxide may therefore have the optimum combination of properties for use in nanocomposites, reasonable stiffness, and strength combined with the presence of reactive functional groups capable of forming a strong interface with the matrix polymer.[12]

CONCLUSIONS

It has been demonstrated that the detailed strain distribution in the graphene monolayer can be mapped in a model composites specimen using Raman spectroscopy, and good stress transfer from the polymer matrix to the graphene monolayer has been demonstrated at matrix strain up to 0.6%. At higher strains fragmentation takes place in the polymer matrix and the interfacial shear stress in the fragments falls to as low as 0.25 MPa, indicating relatively poor adhesion at the graphene−polymer interface. There is clearly a need for more work to be undertaken upon improving the adhesion between the graphene and polymer matrix before the graphene can be employed a reinforcing phase in polymer nanocomposites for structural applications. This study has given a clear demonstration of a technique that can be used to assess the levels of reinforcement in such systems with high precision.

MATERIALS AND METHODS

The specimen was prepared using a 5 mm thick poly(methyl methacrylate) beam spin-coated with 300 nm of cured SU-8 epoxy resin. The graphene was produced by mechanical cleaving of graphite and deposited on the surface of the SU-8. This method produced graphene with a range of different numbers of layers, and the monolayers were identified both optically and by using Raman spectroscopy (see Supporting Information). The PMMA beam was deformed in 4-point bending up to 0.4% strain with the strain monitored using a strain gage attached to the beam surface. Well-defined Raman spectra could be obtained from the graphene monolayer using a low-power HeNe laser (1.96 eV and <1 mW at the sample in a Renishaw 2000 spectrometer), and the deformation of the graphene in the composite was followed from the shift of the 2D (or G′) Raman band. The laser beam polarization was always parallel to the tensile axis, and the spot size of the laser beam on the sample was approximately 2 μm using a 50× objective lens.

Raman spectra were obtained at different strain levels through mapping over the graphene monolayer in steps of between 2 and 5 μm by moving the $x-y$ stage of the microscope manually and checking the position of the laser spot on the specimen relative to the image of the monolayer on the screen of the microscope. The strain at each measurement point was determined from the position of the 2D Raman band using the calibration in Figure 2, and strain maps of the monolayer were produced in the form of colored $x-y$ contour maps using the OriginPro 8.1 graph-plotting software package, which interpolates the strain between the measurement points.

The beam was then unloaded, and a thin 300 nm layer of SU-8 was then spin-coated on top and cured so that the graphene remained visible when sandwiched between the two coated polymer layers. The beam was then reloaded initially up to 0.4% strain, unloaded, and then reloaded to various other levels of strain. The strain in the graphene monolayer was mapped fully at each strain level as well as in the unloaded state.

Acknowledgment. The authors of this work are grateful to the Engineering and Physical Sciences Research Council for support in the form of a Science and Innovation Award (EP/G035954/1). One of the authors (A.S.N.) is also supported by the Royal Society.

Supporting Information Available: (S1) Characterization of the graphene using Raman spectroscopy. (S2) Raman band broadening during the deformation of the graphene monolayer. (S3) Variation of graphene strain along the middle of the

monolayer. (S4) Micrograph of cracking of the specimen surface following deformation. This material is available free of charge via the Internet at http://pubs.acs.org.

REFERENCES AND NOTES

1. Novoselov, K. S.; Geim, A. K.; Morozov, S. V.; Jiang, D.; Zhang, Y.; Dubonos, S. V.; Grigorieva, I. V.; Firsov, A. A. Electric Field Effect in Atomically Thin Carbon Films. *Science* **2004,** *306*, 666–669.
2. Geim, A. K.; Novoselov, K. S. The Rise of Graphene. *Nat. Mater.* **2007,** *6*, 183–190.
3. Novoselov, K. S.; Geim, A. K.; Morozov, S. V.; Jiang, D.; Katsnelson, M. I.; Grigorieva, I. V.; Dubonos, S. V.; Firsov, A. A. Two-Dimensional Gas of Massless Dirac Fermions in Graphene. *Nature* **2005,** *438*, 197–200.
4. Zhang, Y. B.; Tan, Y. W.; Stormer, H. L.; Kim, P. Experimental Observation of the Quantum Hall Effect and Berry's Phase in Graphene. *Nature* **2005,** *438*, 201–204.
5. Geim, A. K. Graphene: Status and Prospects. *Science* **2009,** *324*, 1530–1534.
6. Yu, A. P.; Ramesh, P.; Itkis, M. E.; Bekyarova, E.; Haddon, R. C. Graphite Nanoplatelet-Epoxy Composite Thermal Interface Materials. *J. Phys. Chem. C* **2007,** *111*, 7565–7569.
7. Lee, C.; Wei, X. D.; Kysar, J. W.; Hone, J. Measurement of the Elastic Properties and Intrinsic Strength of Monolayer Graphene. *Science* **2008,** *321*, 385–388.
8. Bunch, J. S.; Verbridge, S. S.; Alden, J. S.; van der Zande, A. M.; Parpia, J. M.; Craighead, H. G.; McEuen, P. L. Impermeable Atomic Membranes from Graphene Sheets. *Nano Lett.* **2008,** *8*, 2458–2462.
9. Kim, H.; Abdala, A. A.; Macosko, C. W. Graphene/Polymer Nanocomposites. *Macromolecules* **2010,** *43*, 6515–6530.
10. Park, S. J.; Ruoff, R. S. Chemical Methods for the Production of Graphenes. *Nat. Nanotechnol.* **2009,** *4*, 217–224.
11. Dreyer, D. R.; Park, S. J.; Bielawski, C. W.; Ruoff, R. S. The Chemistry of Graphene Oxide. *Chem. Soc. Rev.* **2010,** *39*, 228–240.
12. Ramanathan, T.; Abdala, A. A.; Stankovich, S.; Dikin, D. A.; Herrera-Alonso, M.; Piner, R. D.; Adamson, D. H.; Schniepp, H. C.; Chen, X.; Ruoff, R. S.; *et al*. Functionalized Graphene Sheets for Polymer Nanocomposites. *Nat. Nanotechnol.* **2008,** *3*, 327–331.
13. Hummers, W. S.; Offeman, R. E. Preparation of Graphitic Oxide. *J. Am. Chem. Soc.* **1958,** *80*, 1339.
14. Brodie, B. C. On the Atomic Weight of Graphite. *Philos. Trans. R. Soc. London* **1859,** *149*, 249–259.
15. He, H. Y.; Klinowski, J.; Forster, M.; Lerf, A. A New Structural Model for Graphite Oxide. *Chem. Phys. Lett.* **1998,** *287*, 53–56.
16. Wilson, N. R.; Pandey, P. A.; Beanland, R.; Young, R. J.; Kinloch, I. A.; Gong, L.; Liu, Z.; Suenaga, K.; Rourke, J. P.; York, S. J.; *et al*. Graphene Oxide: Structural Analysis and Application as a Highly Transparent Support for Electron Microscopy. *ACS Nano* **2009,** *3*, 2547–2556.
17. Gong, L.; Kinloch, I. A.; Young, R. J.; Riaz, I.; Jalil, R.; Novoselov, K. S. Interfacial Stress Transfer in a Graphene Monolayer Nanocomposite. *Adv. Mater.* **2010,** *22*, 2694–2697.
18. Kelly, A.; Macmillan, N. H. *Strong Solids*, 3rd ed.; Clarendon Press: Oxford, 1986.
19. Nairn, J. A. A Variational Mechanics Analysis of the Stresses around Breaks in Embedded Fibers. *Mech. Mater.* **1992,** *13*, 131–154.
20. Huang, M. Y.; Yan, H.; Chen, C. Y.; Song, D. H.; Heinz, T. F.; Hone, J. Phonon Softening and Crystallographic Orientation of Strained Graphene Studied by Raman Spectroscopy. *Proc. Natl. Acad. Sci.* **2009,** *106*, 7304–7308.
21. Mohiuddin, T. M. G.; Lombardo, A.; Nair, R. R.; Bonetti, A.; Savini, G.; Jalil, R.; Bonini, N.; Basko, D. M.; Galiotis, C.; Marzari, N.; *et al*. Uniaxial Strain in Graphene by Raman Spectroscopy: G Peak Splitting, Gruneisen Parameters, and Sample Orientation. *Phys. Rev. B* **2009,** *79*, 205433.
22. Ferralis, N Probing Mechanical Properties of Graphene with Raman Spectroscopy. *J. Mater. Sci.* **2010,** *45*, 5135–5149.
23. Huang, M. Y.; Yan, H.; Heinz, T. F.; Hone, J. Probing Strain-Induced Electronic Structure Change in Graphene by Raman Spectroscopy. *Nano Lett.* **2010,** *10*, 4074–4079.
24. Ferrari, A. C.; Meyer, J. C.; Scardaci, V.; Casiraghi, C.; Lazzeri, M.; Mauri, F.; Piscanec, S.; Jiang, D.; Novoselov, K. S.; Roth, S.; *et al*. Raman Spectrum of Graphene and Graphene Layers. *Phys. Rev. Lett.* **2006,** *97*, 187401.
25. Malard, L. M.; Pimenta, M. A.; Dresselhaus, G.; Dresselhaus, M. S. Raman Spectroscopy in Graphene. *Phys. Rep.* **2009,** *473*, 51–87.
26. Goh, K. L.; Aspden, R. M.; Mathias, K. J.; Hukins, D. W. L. Finite-Element Analysis of the Effect of Material Properties and Fibre Shape on Stresses in an Elastic Fibre Embedded in an Elastic Matrix in a Fibre−Composite Material. *Proc. R. Soc. London A* **2004,** *460*, 2339–2352.
27. Goh, K. L.; Meakin, J. R.; Hukins, D.W. L. Influence of Fibre Taper on the Interfacial Shear Stress in Fibre-Reinforced Composite Materials during Elastic Stress Transfer. *Compos. Interfaces* **2010,** *17*, 75–81.
28. Kinloch, A. J.; Young, R. J. *Fracture Behaviour of Polymers*; Applied Science Publishers: London, 1983.
29. Huang, Y. L.; Young, R. J. Analysis of the Fragmentation Test for Carbon-Fiber Epoxy Model Composites by Means of Raman Spectroscopy. *Compos. Sci. Technol.* **1994,** *52*, 505–517.
30. van den Heuvel, P. W. J.; Peijs, T.; Young, R. J. Failure Phenomena in Two-Dimensional Multi-Fibre Microcomposites. 2. A Raman Spectroscopic Study of the Influence of Inter-Fibre Spacing on Stress. *Compos. Sci. Technol.* **1997,** *57*, 899–911.
31. Chowdhury, M. C.; Okabe, T. Computer Simulation of Carbon Nanotube Pull-Out from Polymer by the Molecular Dynamics Method. *Composites, Part A* **2007,** *38*, 747–754.
32. Awasthi, A. P.; Lagoudas, D. C.; Hammerand, D. C. Modeling of Graphene-Polymer Interfacial Mechanical Behavior using Molecular Dynamics. *Model. Simul. Mater. Sci. Eng.* **2009,** *17*, 015002.
33. Bangert, U.; Gass, M. H.; Bleloch, A. L.; Nair, R. R.; Eccles, J. Nanotopography of Graphene. *Phys. Status Solidi A* **2009,** *206*, 2115–2119.
34. Gómez-Navarro, C.; Meyer, J. C.; Sundaram, R. S.; Chuvilin, A.; Kurasch, S.; Burghard, M.; Kern, K.; Kaiser, U. Atomic Structure of Reduced Graphene Oxide. *Nano Lett.* **2010,** *10*, 1144–1148.
35. Erickson, K.; Erni, R.; Lee, Z. H.; Alem, N.; Gannett, W.; Zettl, A. Determination of the Local Chemical Structure of Graphene Oxide and Reduced Graphene Oxide. *Adv. Mater.* **2010,** *22*, 4467–4472.
36. Gomez-Navarro, C.; Burghard, M.; Kern, K. Elastic Properties of Chemically Derived Single Graphene Sheets. *Nano Lett.* **2008,** *8*, 2045–2049.
37. Suk, J. W.; Piner, R. D.; An, J.; Ruoff, R. S. Mechanical Properties of Monolayer Graphene Oxide. *ACS Nano* **2010,** *4*, 6557–6564.